ACS Macro Letters

pubs.acs.org/macroletters Letter

Synthesis of Polymer Nanoweb via a Lipid Template

Chung-Hao Liu, Susan Krueger, and Mu-Ping Nieh*

Cite This: ACS Macro Lett. 2023, 12, 993−998 Read Online

ACCESS | Metrics & More | Article Recommendations | Supporting Information

ABSTRACT: We report a generalized platform for synthesizing a polymer nanoweb with a high specific surface area via a bicellar template, composed of 1,2-dipalmitoyl phosphocholine (DPPC), 1,2-dihexanoyl phosphocholine (DHPC), and 1,2-dipalmitoyl phosphoglycerol (DPPG). The pristine bicelle (in the absence of monomer or polymer) yields a variety of well-defined structures, including disc, vesicle, and perforated lamella. The addition of styrene monomers in the mixture causes bicelles to transform into lamellae. Monomers are miscible with DPPC and DPPG initially, while polymerization drives polymers to the DHPC-rich domain, resulting in a polymer nanoweb supported by the outcomes of small angle neutron scattering, differential scanning calorimetry, and transmission electron microscopy.

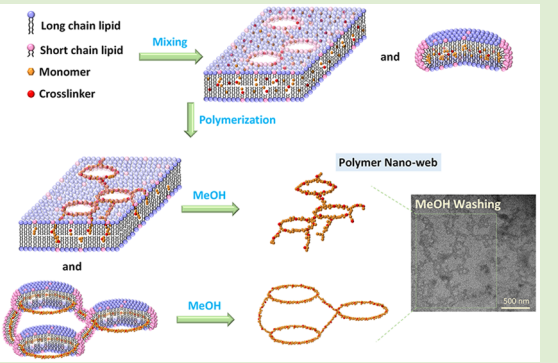

Interpenetrating polymer networks (IPNs) have many applications, such as hydrogels,[1,2] drug delivery systems, etc.[3,4] Usually, IPNs are synthesized from two different polymers that are physically entangled but not chemically bonded.[3,5] The numerous studies, such as silicon-based, polyisoprene, or copolymer networks, have been published in several decades.[6,7] IPNs are typically classified into simultaneous IPN (sim-IPN), sequential IPN (seq-IPN), and semi-IPN by their synthetic routes or the physical arrangement of polymers.[8,9] The sim-IPN involves polymerization with two mixing monomers in the presence of appropriate catalysts and cross-linkers, while seq-IPN is synthesized via a multistage sequential process. However, phase separation may take place during the reactions because of low polymer miscibility. IPNs have several advantages such as a high porosity structure with interconnected networks, a high permeability, and a large surface area.[10] Lumelsky et. al utilized polymerized HIPEs (polyHIPEs) to synthesize polycaprolactone diol, producing voids on the order of hundreds of microns which is appropriate for tissue engineering.[11] Lépine et. al simultaneously used radical and step-growth polymerization to synthesize polyurethane-polystyrene network via IPN polyHIPEs.[12] Recently, Israel et. al found that the formation of interconnected networks from hyper-cross-linking an IPN synthesized with an aromatic diisocyanate enhanced the microporosity as well as thermal stability.[13] Nevertheless, the emulsions are thermodynamically unstable[14,15] and may undergo phase separation.[10] In addition, high temperatures are usually needed when carrying out step-growth polymerization in the polyHIPEs approach.[10,13]

Previous reports have shown syntheses of polymer disks, porous polymer, and polymer nanorings are achievable through emulsion polymerization via a stable lipid template, known as bicelles or liposomes.[16−18] Such lipid mixtures can yield well-defined and stable discoidal bicelles,[19] unilamellar vesicles (ULVs),[20] multilamellar vesicles (MLVs), perforated lamellae,[21,22] or bilayered ribbons[23,24] strongly depending on lipid concentrations,[25] temperature,[21,26] charged lipid ratio,[25] and molecular archiecture.[27] One of the most studied lipid mixtures contains long-chain zwitterionic dipalmitoylphosphatidylcholine (DPPC), anionic dipalmitoylphosphatidylglycerol (DPPG), and short-chain zwitterionic dihexanoylphosphatidylcholine (DHPC), and their chemical structures are shown in Figure 1. It has been reported that the molar ratio of long-chain lipids to short-chain lipids between 2 and 5 can generate a uniform bicelle. A higher charge density, i.e., higher DPPG-to-total lipid ratio, is also important for enhancing the stability of discoidal bicelles.[19,26] Here, we utilized the same compositions of DPPC, DHPC, and DPPG as our previous report, which showed stable bicelles even after styrene- or polystyrene-encapsulation.[16] Their spontaneous morphology is dictated by hydrophobic interactions, segregation of gel-phase and fluid-phase lipids, spontaneous molecular curvatures, mismatch in aqueous solubility between long- and short-chain lipids, and surface charge density.[19] Using this bicellar template, a well-defined polystyrene nanoring is attainable in an aqueous solution as (styrene monomer + divinylbenzene cross-linker)-to-lipid, ([S]+[DVB])/[L], molar ratio ≤ 0.05,

Received: May 1, 2023
Accepted: June 29, 2023

https://doi.org/10.1021/acsmacrolett.3c00255
ACS Macro Lett. 2023, 12, 993−998

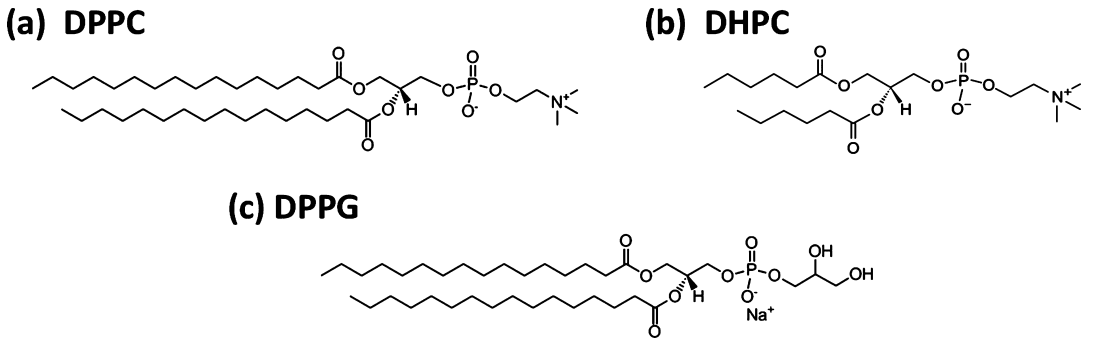

Figure 1. Chemical structures of (a) DPPC, (b) DHPC, and (c) DPPG.

Table 1. Advantages and Challenges of Interpenetrating Polymer Networks (IPNs), Polymerized High Internal Phase Emulsions (polyHIPEs), and a Lipid Template

synthetic approaches	advantages	challenges
interpenetrating polymer networks (IPNs)	• The polymer networks have strong mechanical properties and high stability.[36]	• Phase separation can take place during the polymerization, leading to a broad spectrum of domain compositions.[8]
	• The strategy is commonly used to generate hydrogel, shape memory, energy storage, biorelated fields, etc.[37,38]	
polymerized high internal phase emulsions (polyHIPEs)	• Functionalization of the polyHIPEs surfaces for postpolymerization reactions is possible.[39]	• The emulsions are not thermodynamically stable.[14,15]
	• It is commonly used for scaffolds in tissue engineering, prolong drug release, catalytic reaction, etc.[11,39,40]	• High temperature is needed for step-growth polymerization.[10,13]
lipid template	• It provides a stable and green process.	• The cost of materials for large-scale manufacturing is relatively high presently.
	• The synthesis is robust and the morphology can be well controlled.	
	• It is a generalized platform for other hydrophobic monomers.[16]	

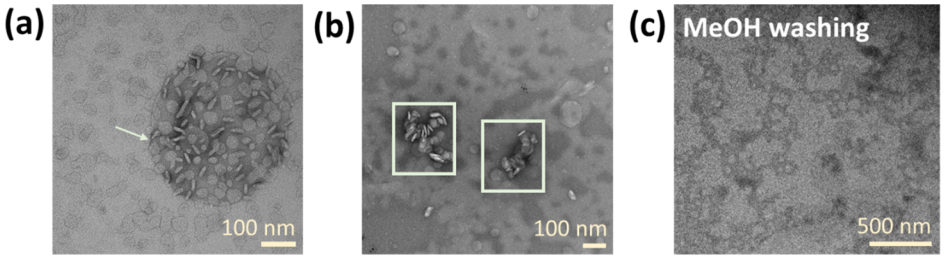

Figure 2. (a, b) TEM micrograms of 0.003 wt % PS/L as the polymerization performed at C_{lp} = 10 wt % (negatively stained). (c) The TEM micrograph of PS after the removal of lipids via methanol washes without being negatively stained.

and this strategy is proven applicable for multiple hydrophobic vinyl monomers.[16]

Here, we report that a model monomer, styrene, and a cross-linker, divinylbenzene (DVB) can generate polymer nanoweb, instead of nanorings, when ([S] + [DVB])/[L] ratio is above 0.1 in DPPC/DHPC/DPPG system. Two important findings include (1) morphological transformation from discoidal bicelles to lamellae upon the addition of overwhelming styrene monomers, and (2) formation of polystyrene nanoweb after removal of the lipid scaffold as confirmed by small angle neutron scattering (SANS), differential scanning calorimetry (DSC), transmission electron microscopy (TEM), atomic force microscopy (AFM), and scanning electron microscopy (SEM). As compared to conventional methods (IPNs[3,5] or polyHIPEs[10,28]), this approach is more straightforward and environmentally friendly to form a highly porous polymer nanoweb at room temperature (Table 1). This novel strategy can be further extended to other hydrophobic monomers for manufacturing functional polymer nanoweb for the applications of nanomedicine,[29−31] protein separation, gas separation, batteries, or fuel cells in the future.[32−35]

The small-angle X-ray scattering (SAXS) patterns of polymerized S/L (PS/L) as 0.10 ≤ ([S] + [DVB])/[L] ≤ 0.33 contain two characteristic features: a group of Bragg peaks (q_1*, $2q_1$*, $3q_1$*, etc.) representing a lamellar structure and three broad peaks in the q range from 0.05 to 0.5 Å^{-1} reflecting a phospholipid bilayered structure as shown in Figure S1(a). However, samples of high ([S] + [DVB])/[L] values show phase separation after preparation, while the ([S] + [DVB])/[L] = 0.1 sample sits at the boundary between discoidal bicelles and lamellae [Figure S1(b)]. Our discussion will focus on PS/L with ([S] + [DVB])/[L] = 0.2. Hereafter, S/L and PS/L are referred to as before and after polymerization, respectively, for 0.2. Figure 2a,b shows the negative staining transmission electron microscopic (ns-TEM) micrographs of the PS/L mixture with a lipid concentration (C_{lp}) diluted to 0.003 wt %, though being polymerized at C_{lp} = 10 wt %. Note that the completion of polymerization is confirmed by Figure S2. Well-defined discoidal bicelles are found confined to each

https://doi.org/10.1021/acsmacrolett.3c00255
ACS Macro Lett. 2023, 12, 993−998

other, forming spherical aggregates (Figure 2a) or in stacks (Figure 2b) through invisible "strings". This outcome differs from the previous report, where PS/L with ([S] + [DVB])/[L] ≤ 0.05 showed well-dispersed bicelles.[16] The "stringing" behavior becomes evident after removal of the lipid template through methanol washing. The TEM micrograph (Figure 2c) demonstrates interconnected PS nanoweb populated with "hollow" discs, suggesting that PS connects these discs in an aqueous solution. The blurry image of Figure 2c comes from the weak contrast between the PS and the environment.

This observation intrigues us to study deuterated styrene/lipid (*d*S/L) and polymerized *d*S/L (*d*PS/L) mixtures using contrast-matched (CM) small-angle neutron scattering (SANS), where the neutron scattering length density (NSLD) of solvent ($\rho_{solvent}$) matches the average NSLD of lipids and *d*S ($\rho_{dS/L}$). This approach minimizes the contribution from "structure factor" (i.e., interparticle interaction) and thus enhances the scattering mainly from *d*S or *d*PS, allowing us to envision the detailed structure of the template. Figure 3a presents the CM-SANS data of *d*S/L and

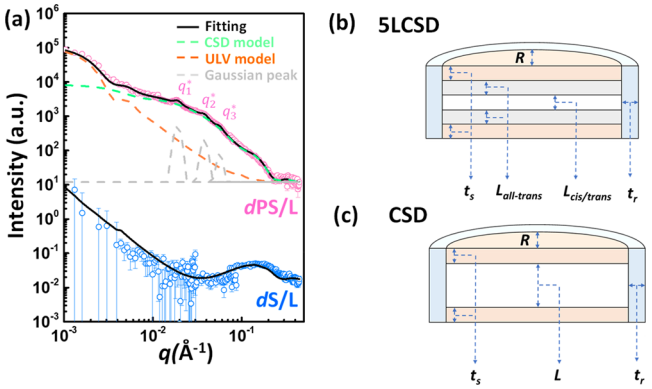

Figure 3. (a) CM SANS patterns of *d*S/L and *d*PS/L, as polymerization performed at C_{lp} of 10.0 wt %. (b) The scheme of the 5LCSD model. The *R*, t_s, t_r, $L_{all\text{-}trans}$, and $L_{cis/trans}$ are core radius, shell thickness, rim thickness, thicknesses of all-trans and cis/trans coexisting layers, respectively. (c) The scheme of the CSD model. The *R*, t_s, t_r, and *L* are core radius, shell thickness, rim thickness and hydrophobic thickness, respectively. Note that schemes in (b) and (c) do not reflect the dimensional ratios of the nanodiscs.

*d*PS/L showing distinct patterns. However, SANS of both samples in D_2O (revealing the global, instead of internal, structure) instead of CM-water, shown in Figure S3(a), are similar to high-order Bragg peaks (up to fourth-order or more), suggesting a lamellar structure, consistent with the SAXS results [Figure S3(b)]. Evidently, introduction of styrene into bicelles results in a structural transformation from bicelle to lamella, which is only observed as temperature (*T*) is higher than the melting temperature (T_m) of long-chain lipid (in this case, DPPC) or insufficient short-chain lipid (in this case, DHPC) for high-C_{lp} samples in absence of styrene.[21,22,26,27] In fact, the reduced T_m of DPPC in the *d*S/L mixture [~26.6 °C; Figure S3(c)] indicates *d*S mixes well with DPPC and justifies the formation of lamellae, while the lamellae expectedly retained even after polymerization where T_m was restored (~41.8 °C), as shown in Figure S3(d). The CM-SANS data show that *d*S/L is better contrast-matched than *d*PS/L (Figure 2a), suggesting that styrene is more miscible with the DPPC, also consistent with the above-mentioned DSC outcomes of lower T_m of DPPC for *d*S/L (~26.6 °C) compared to that of *d*PS/L [~41.8 °C; Figure S3(d)]. This observation agrees with the previous report for samples with lower S/L ratios.[16] Furthermore, the fact that Bragg peaks appear in the CM-SANS data of *d*PS/L, instead of *d*S/L data (Figure 3a), indicates breaking of the CM condition due to the demixing of *d*PS from DPPC. For the *d*S/L system, we utilized a recently developed five-layer core−shell discoidal model (5LCSD, Figure 3b and Supporting Information),[41] which describes the bilayer neutron scattering density (NSLD) profile as phosphate-all trans−trans/cis−all trans-phosphate (Figure 3b) across the bilayer, to best-fit the CM-SANS data (Figure 3a). The best fitting structural parameters are listed in Table 2. An

Table 2. Best Fitting Results of *d*S/L and *d*PS/L

*d*S/L		*d*PS/L	
5LCSD model		CSD model	
R (Å)	>2000	*R* (Å)	180 ± 3
t_r (Å)	100 ± 80	t_r (Å)	65 ± 1
t_s (Å)	10 ± 2	t_s (Å)	12 ± 1
$L_{all\text{-}trans}$ (Å)	8 ± 1	*L* (Å)	27 ± 1
$L_{cis/trans}$ (Å)	5 ± 1	ρ_{core} (×10^{-6} Å^{-2})	−0.74 ± 0.03
$\rho_{all\text{-}trans}$ (×10^{-6} Å^{-2})	−0.4 ± 0.1	ρ_{rim} (×10^{-6} Å^{-2})	1.3 ± 0.02
$\rho_{cis/trans}$ (×10^{-6} Å^{-2})	−0.03 ± 0.1		
ρ_{rim} (×10^{-6} Å^{-2})	0.4 ± 0.1		
		ULV model	
		R (Å)	730 ± 13
		t_b (Å)	35 ± 2

intriguing discovery is that the NSLD of the cis/trans coexisting regime (central layer of the bilayer), $\rho_{cis/trans}$ is -0.03×10^{-6} Å^{-2} higher than that of the ordered chain, $\rho_{all\text{-}trans}$ (-0.4×10^{-6} Å^{-2}), implying *d*S monomers may preferably locate at the center disordered layer, which is similar to the previous report.[42]

After polymerization, the ns-TEM suggests that the low-C_{lp}*d*PS/L sample contains both discoidal bicelles and vesicles (Figure 2); a proper scattering model should combine discoidal and vesicular scattering functions for data fitting. It should be noted that the attempt of using a unilamellar vesicle (ULV) model alone to fit the scattering patterns was not successful, as the best fit completely misses the mid- and high-*q* data (the orange dashed line in Figure 3a). The oscillation at the low-*q* represents ULVs, yielding an average best-fit radius (*R*) of 730 (±13) Å and bilayer thickness (t_b) of 35(±2) Å (Table 2). The scattering data at $q > 0.007$ Å^{-1} can be best described as the core−shell discoidal (CSD) model[43] (the green dashed line in Figure 3a) with a core radius (R_c) of 180(±3) Å, rim thickness (t_r) of 65(±1), and hydrophobic thickness (*L*) of 27(±1) Å (Table 2). The best fitting volume fraction ratio of discoidal bicelles to vesicles is around 1:3.7. Note that the SANS of *d*PS/L was best fitted by the CSD model because the cis/trans and all-trans regimes are indistinguishable after polymerization. Three quasi-Bragg peaks located at q = 0.0188 Å^{-1}, 0.0374 Å^{-1}, and 0.0565 Å^{-1} correspond to the first-, second-, and third-order harmonics, [q_1*, q_2* (=2q_1*), and q_3* (=3q_1*), respectively] from stacking lamellar structures. Therefore, we incorporated three Gaussian peaks at q_1*, 2q_1*, and 3q_1* (the gray dashed line in Figure 3a) in the best-fitting model to describe the repeat spacing of the lamellae. It is noteworthy that the best fitting NSLD at rim, ρ_{rim}, increases from 0.4 (±0.1) × 10^{-6} Å^{-2} in *d*S/L to 1.3(±0.02) × 10^{-6} Å^{-2} in *d*PS/L, suggesting that *d*PS

https://doi.org/10.1021/acsmacrolett.3c00255
ACS Macro Lett. 2023, 12, 993−998

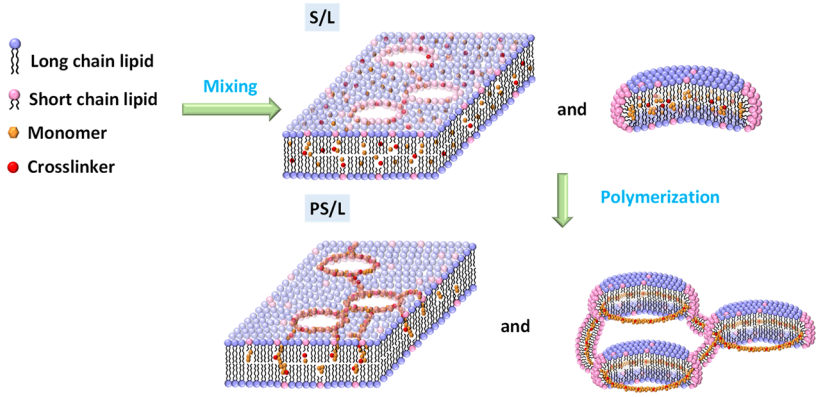

Figure 4. Schematic representation of the styrene monomers and DVB cross-linkers in the lipid templates (S/L) and its polymerization (PS/L). At the beginning, monomers and cross-linkers homogeneously distribute in the lamellae and discoidal bicelles. After polymerization, the PS populate in the fluid phase, which further extends and connects along the DHPC defects, forming the PS nanoweb, as confirmed by SANS and microscopy results.

preferably locates at the DHPC-rich fluid rim. In other words, polystyrene extends and connects along DHPC defects in discoidal bicelles or lamellae and thus forms the polymer nanoweb. The TEM of lipid-removed PS/L showing many "empty" circles agrees with such a proposed structure. Figure S3(d) provides further evidence of the immiscibility between PS and DPPC as the T_m of the PS/L reverted to that in the pristine bicelles (PB). The formation mechanism will be further discussed in the following section.

In addition, we observed a distinct difference in the property of S/L lamellae in comparison with the perforated lamellae of the pristine bicellar mixture at high T, where dilution of the system results in $1 - D$ swelling, i.e., $D \sim C_{lp}^{-1}$.[21,22,25,27] The swelling of S/L lamellae is, however, highly constrained with a scaling of $D \sim C_{lp}^{-0.56}$ (Figure S4 and Table S1). This can be attributed to the following possible reasons: (1) lamellae are not homogeneously dispersed in the solution, (2) the lateral lipid density on the lamellae decreases upon dilution, and (3) the number of lamellae increases upon dilution (Figures S4–S6 and Tables S1 and S2).

Upon polymerization, styrene and DVB are continuously drawn to the DHPC-rich domain, forming cross-linked PS, as illustrated in Figure 4. The high-C_{lp} system is presumably a morphological mixture of bicellar discs and perforated lamellae (some of them possibly constituting the shell of the vesicles), with PS shielded by DHPC, as previously reported in similar systems at lower S/L ratios.[16] However, the large-quantity PS in the current PS/L system further extends and connects (either in the bilayer to minimize the hydrophobic mismatch between DHPC and DPPC or through the aqueous phase) to the nearby PS residing in the DHPC-rich defects, eventually forming interconnected three-dimensional "webs", as confirmed by TEM (Figure 2), AFM (Figure S7), and SEM (Figure S8) after removing lipids.

We are able to use the Gibbs free energy of mixing, $\Delta\bar{G}_m$, to explain the formation mechanism of nanoweb.

$$\Delta\bar{G}_m = kT\left[\frac{\phi}{N_P}\ln\phi + \frac{1-\phi}{N_S}\ln(1-\phi) + \chi\phi(1-\phi)\right] \quad (1)$$

where k, ϕ, N_P, N_S, and χ are Boltzmann constant, volume fraction of the polymer, the degree of polymerization, the repeat unit of solvent molecules, and the Flory–Huggins interaction parameter, respectively. The first two terms are entropic terms, while the last term represents the energetic term of mixing. After polymerization, N_P increases, causing decreased entropy of mixing. As the N_S of DPPC is larger than that of DHPC, it is expected that PS would prefer to reside in the DHPC-rich disordered phase (increased entropy). The depletion of polymers effectively promotes the formation of DPPC liquid ordered phase, which has a lower χ than the disordered DPPC containing PS does. The higher melting enthalpy of DPPC for PS/L than that for S/L [Figure S3(d)] further supports our hypothesis. The polymerization induced segregation between PS and DPPC was previously reported in the lower S-to-L ratios.[16] The fact that the discs are not dissociated from each other after dilution into C_{lp} = 0.003 wt %, but form aggregates as shown in Figure 2a,b, also suggests that PS "strings" discs together possibly through the PS at the rim. The observed empty circles in the TEM (Figure 2c) agree with such a presumption.

The current platform can be generalized for synthesis of cross-linked polymer nanoweb using other hydrophobic monomers. It should be noted that the mesh size, in principle, is expectedly adjustable by the following controlling parameters: ([S] + [DVB])/[L], the ratio of long-chain to short-chain lipids and C_{lp}. The polymer network has the advantages of robustness and potential generalization for various polymers compared to those achieved through IPNs and IPN polyHIPE.[3,5,28] Here, the approach is a facile and ecofriendly synthesis to generate a polymer nanoweb following the sequence of well-defined self-assembly platform→ polymerization → removal of the lipid template.

This approach enriches the strategies of polymer synthesis in a more controlled manner by green chemistry.[44] Furthermore, functional and highly cross-linked polymer network is attainable through the thiol–ene "click chemistry"[32] (e.g., using equimolar –SH and C=C groups) under an ambient environment.[45] The interface area can be greatly enhanced for catalytic reactions,[39] shape-memory materials,[46] tissue-engineering scaffolds,[11,47] studies of the drug release mechanism,[40] and adsorption and absorption applications[48,49] for future applications.

https://doi.org/10.1021/acsmacrolett.3c00255
ACS Macro Lett. 2023, 12, 993–998

■ ASSOCIATED CONTENT

Supporting Information

The Supporting Information is available free of charge at https://pubs.acs.org/doi/10.1021/acsmacrolett.3c00255.

Further details of sample preparation, the descriptions of scattering models, and additional of figures and tables (PDF)

■ AUTHOR INFORMATION

Corresponding Author

Mu-Ping Nieh − *Polymer Program, Institute of Materials Science, University of Connecticut, Storrs, Connecticut 06269, United States; Department of Chemical and Biomolecular Engineering, University of Connecticut, Storrs, Connecticut 06269, United States;* orcid.org/0000-0003-4462-8716; Email: mu-ping.nieh@uconn.edu

Authors

Chung-Hao Liu − *Polymer Program, Institute of Materials Science, University of Connecticut, Storrs, Connecticut 06269, United States*

Susan Krueger − *Center for Neutron Research, National Institute of Standard and Technology, Gaithersburg, Maryland 20899, United States*

Complete contact information is available at: https://pubs.acs.org/10.1021/acsmacrolett.3c00255

Author Contributions

C.-H.L. formulated the concept, collected all the scattering data and DSC data, performed the data analysis, and composed the first edition of this Letter. S.K. set up the SANS configurations and performed the sample measurements for this project. M.-P.N. oversaw the whole project.

Notes

Access to SANS was provided by the Center for High Resolution Neutron Scattering, a partnership between the National Institute of Standards and Technology and the National Science Foundation under Agreement No. DMR-2010792. Certain commercial equipment, instruments, or materials (or suppliers, or software, ...) are identified in this paper to foster understanding. Such identification does not imply recommendation or endorsement by the National Institute of Standards and Technology, nor does it imply that the materials or equipment identified are necessarily the best available for the purpose.

The authors declare no competing financial interest.

■ ACKNOWLEDGMENTS

C.-H.L. and M.-P.N. would like to acknowledge NSF (CBET 1930906) for the partial support for the project. The authors thank Drs. Hao Ding and Zaili Huo for atomic force microscopy (AFM) and scanning electron microscopy (SEM) measurements, respectively. We also thank Dr. Lin Yang and the beamtime of 16ID-LiX at the NSLS-II (Brookhaven National Lab) through a beamtime proposal (BAG-302208). The LiX beamline is part of the Center for BioMolecular Structure (CBMS), which is primarily supported by the National Institutes of Health, National Institute of General Medical Sciences (NIGMS) through a P30 Grant (P30GM133893), and by the DOE Office of Biological and Environmental Research (KP1605010). LiX also received additional support from NIH Grant S10 OD012331. As part of NSLS-II, a national user facility at Brookhaven National Laboratory, work performed at the CBMS is supported in part by the U.S. Department of Energy, Office of Science, Office of Basic Energy Sciences Program under Contract Number DE-SC0012704. Access to SANS was provided by the Center for High Resolution Neutron Scattering, a partnership between the National Institute of Standards and Technology and the National Science Foundation under Agreement No. DMR-2010792.

■ REFERENCES

(1) Ishikawa, S.; Iijima, K.; Matsukuma, D.; Asawa, Y.; Hoshi, K.; Osawa, S.; Otsuka, H. Interpenetrating Polymer Network Hydrogels via a One-Pot and in Situ Gelation System Based on Peptide Self-Assembly and Orthogonal Cross-Linking for Tissue Regeneration. *Chem. Mater.* **2020**, *32* (6), 2353−2364.

(2) Yang, D. Recent Advances in Hydrogels. *Chem. Mater.* **2022**, *34* (5), 1987−1989.

(3) Dragan, E. S. Design and applications of interpenetrating polymer network hydrogels. A review. *Chemical Engineering Journal* **2014**, *243*, 572−590.

(4) Manna, S.; Manna, M.; Jana, S., Interpenetrating Polymer Network in Microparticulate Systems: Drug Delivery and Biomedical Application. In *Interpenetrating Polymer Network: Biomedical Applications*, Jana, S., Jana, S., Eds.; Springer: Singapore, 2020; pp 1−23.

(5) Sperling, L. H.; George, H. F.; Huelck, V.; Thomas, D. A. Viscoelastic behavior of interpenetrating polymer networks: Poly-(ethyl acrylate)-poly(methyl methacrylate). *J. Appl. Polym. Sci.* **1970**, *14* (11), 2815−2824.

(6) Staudinger, H.; Fritschi, J. Über Isopren und Kautschuk. 5. Mitteilung. Über die Hydrierung des Kautschuks und über seine Konstitution. *Helv. Chim. Acta* **1922**, *5* (5), 785−806.

(7) Staudinger, H.; Heuer, W. Über hochpolymere Verbindungen, 94. Mitteil.: Über ein unlösliches Poly-styrol. *Berichte der deutschen chemischen Gesellschaft (A and B Series)* **1934**, *67* (7), 1164−1172.

(8) Silverstein, M. S. Interpenetrating polymer networks: So happy together? *Polymer* **2020**, *207*, 122929.

(9) Beebe, J. M.; Ahn, D.; Eldred, D. V.; Fielitz, A. J.; Heyl, T. R.; Lee, M.; Mangold, S.; Pearce, E. Z.; Reinhardt, C. W.; Roggenbuck, C.; Scherzer, J. M.; Shull, K. R.; Silvaroli, A. J.; Tan, Y.-J.; Wang, M. Photocured Simultaneous and Sequential PDMS/PMMA Interpenetrating Polymer Networks. *Macromolecules* **2022**, *55* (13), 5826−5839.

(10) Zhang, T.; Sanguramath, R. A.; Israel, S.; Silverstein, M. S. Emulsion Templating: Porous Polymers and Beyond. *Macromolecules* **2019**, *52* (15), 5445−5479.

(11) Lumelsky, Y.; Zoldan, J.; Levenberg, S.; Silverstein, M. S. Porous Polycaprolactone-Polystyrene Semi-interpenetrating Polymer Networks Synthesized within High Internal Phase Emulsions. *Macromolecules* **2008**, *41* (4), 1469−1474.

(12) Lépine, O.; Birot, M.; Deleuze, H. Preparation of macrocellular PU-PS interpenetrating networks. *Polymer* **2005**, *46* (23), 9653−9663.

(13) Israel, S.; Levin, M.; Oliel, S.; Mayer, D.; Lerner, I.; Silverstein, M. S. Hierarchical Porosity in Emulsion-Templated, Porogen-Containing Interpenetrating Polymer Networks: Hyper-Cross-Linking and Carbonization. *Macromolecules* **2022**, *55* (6), 1992−2002.

(14) Hu, M.; Russell, T. P. Polymers with advanced architectures as emulsifiers for multi-functional emulsions. *Materials Chemistry Frontiers* **2021**, *5* (3), 1205−1220.

(15) Lovell, P. A.; Schork, F. J. Fundamentals of Emulsion Polymerization. *Biomacromolecules* **2020**, *21* (11), 4396−4441.

(16) Liu, C.-H.; Cheu, C.; Barker, J. G.; Yang, L.; Nieh, M.-P. Facile polymerization in a bicellar template to produce polymer nano-rings. *J. Colloid Interface Sci.* **2023**, *630*, 629−637.

(17) Tekobo, S.; Pinkhassik, E. Directed covalent assembly of rigid organic nanodisks using self-assembled temporary scaffolds. *Chem. Commun.* **2009**, No. 9, 1112−1114.

(18) Danila, D. C.; Banner, L. T.; Karimova, E. J.; Tsurkan, L.; Wang, X.; Pinkhassik, E. Directed Assembly of Sub-Nanometer Thin Organic Materials with Programmed-Size Nanopores. *Angew. Chem., Int. Ed.* **2008**, *47* (37), 7036−7039.
(19) Liu, Y.; Xia, Y.; Rad, A. T.; Aresh, W.; Nieh, M.-P., Stable Discoidal Bicelles: A Platform of Lipid Nanocarriers for Cellular Delivery. In *Liposomes: Methods and Protocols*, D'Souza, G. G. M., Ed.; Springer: New York, NY, 2017; pp 273−282.
(20) Nieh, M.-P.; Dolinar, P.; Kučerka, N.; Kline, S. R.; Debeer-Schmitt, L. M.; Littrell, K. C.; Katsaras, J. Formation of Kinetically Trapped Nanoscopic Unilamellar Vesicles from Metastable Nanodiscs. *Langmuir* **2011**, *27* (23), 14308−14316.
(21) Nieh, M.-P.; Raghunathan, V. A.; Pabst, G.; Harroun, T.; Nagashima, K.; Morales, H.; Katsaras, J.; Macdonald, P. Temperature Driven Annealing of Perforations in Bicellar Model Membranes. *Langmuir* **2011**, *27* (8), 4838−4847.
(22) Nieh, M.-P.; Glinka, C. J.; Krueger, S.; Prosser, R. S.; Katsaras, J. SANS Study of the Structural Phases of Magnetically Alignable Lanthanide-Doped Phospholipid Mixtures. *Langmuir* **2001**, *17* (9), 2629−2638.
(23) Nieh, M.-P.; Raghunathan, V. A.; Glinka, C. J.; Harroun, T. A.; Pabst, G.; Katsaras, J. Magnetically Alignable Phase of Phospholipid "Bicelle" Mixtures Is a Chiral Nematic Made Up of Wormlike Micelles. *Langmuir* **2004**, *20* (19), 7893−7897.
(24) Soong, R.; Nieh, M.-P.; Nicholson, E.; Katsaras, J.; Macdonald, P. M. Bicellar Mixtures Containing Pluronic F68: Morphology and Lateral Diffusion from Combined SANS and PFG NMR Studies. *Langmuir* **2010**, *26* (4), 2630−2638.
(25) Nieh, M.-P.; Glinka, C. J.; Krueger, S.; Prosser, R. S.; Katsaras, J. SANS Study on the Effect of Lanthanide Ions and Charged Lipids on the Morphology of Phospholipid Mixtures. *Biophys. J.* **2002**, *82* (5), 2487−2498.
(26) Liu, Y.; Li, M.; Yang, Y.; Xia, Y.; Nieh, M.-P. The effects of temperature, salinity, concentration and PEGylated lipid on the spontaneous nanostructures of bicellar mixtures. *Biochimica et Biophysica Acta (BBA) - Biomembranes* **2014**, *1838* (7), 1871−1880.
(27) Li, M.; Heller, W. T.; Liu, C.-H.; Gao, C. Y.; Cai, Y.; Hou, Y.; Nieh, M.-P. Effects of fluidity and charge density on the morphology of a bicellar mixture - A SANS study. *Biochimica et Biophysica Acta (BBA) - Biomembranes* **2020**, *1862* (9), 183315.
(28) Cameron, N. R.; Sherrington, D. C., High internal phase emulsions (HIPEs) − Structure, properties and use in polymer preparation. *Biopolymers Liquid Crystalline Polymers Phase Emulsion*; Springer: Berlin, Heidelberg, 1996; pp 163−214.
(29) Blackman, L. D.; Varlas, S.; Arno, M. C.; Houston, Z. H.; Fletcher, N. L.; Thurecht, K. J.; Hasan, M.; Gibson, M. I.; O'Reilly, R. K. Confinement of Therapeutic Enzymes in Selectively Permeable Polymer Vesicles by Polymerization-Induced Self-Assembly (PISA) Reduces Antibody Binding and Proteolytic Susceptibility. *ACS Central Science* **2018**, *4* (6), 718−723.
(30) Mane, S. R.; Sathyan, A.; Shunmugam, R. Barbiturate derived amphiphilic homopolymers: synthesis, characterization, self-assembly and anticancer drug delivery. *Therapeutic Delivery* **2019**, *10* (7), 419−431.
(31) Couturaud, B.; Georgiou, P. G.; Varlas, S.; Jones, J. R.; Arno, M. C.; Foster, J. C.; O'Reilly, R. K. Poly(Pentafluorophenyl Methacrylate)-Based Nano-Objects Developed by Photo-PISA as Scaffolds for Post-Polymerization Functionalization. *Macromol. Rapid Commun.* **2019**, *40* (2), 1800460.
(32) Kolb, H. C.; Finn, M. G.; Sharpless, K. B. Click Chemistry: Diverse Chemical Function from a Few Good Reactions. *Angew. Chem., Int. Ed.* **2001**, *40* (11), 2004−2021.
(33) Biener, J.; Stadermann, M.; Suss, M.; Worsley, M. A.; Biener, M. M.; Rose, K. A.; Baumann, T. F. Advanced carbon aerogels for energy applications. *Energy Environ. Sci.* **2011**, *4* (3), 656−667.
(34) Sun, N.; Lu, F.; Yu, Y.; Su, L.; Gao, X.; Zheng, L. Alkaline Double-Network Hydrogels with High Conductivities, Superior Mechanical Performances, and Antifreezing Properties for Solid-State Zinc-Air Batteries. *ACS Appl. Mater. Interfaces* **2020**, *12* (10), 11778−11788.
(35) Fan, L.-Z.; Hu, Y.-S.; Maier, J.; Adelhelm, P.; Smarsly, B.; Antonietti, M. High Electroactivity of Polyaniline in Supercapacitors by Using a Hierarchically Porous Carbon Monolith as a Support. *Adv. Funct. Mater.* **2007**, *17* (16), 3083−3087.
(36) Purkait, M. K.; Sinha, M. K.; Mondal, P.; Singh, R., Chapter 3 - Temperature-Responsive Membranes. In *Interface Science and Technology*, Purkait, M. K., Sinha, M. K., Mondal, P., Singh, R., Eds.; Elsevier, 2018; Vol. *25*, pp 67−113.
(37) Zhou, C.; Yuan, S.; Dai, T.; Zhou, S.; Zou, H.; Liu, P. Environment-adaptable PAM/PVA Semi-IPN hydrogels reinforced by GO for high electromagnetic shielding performance. *Polymer* **2022**, *253*, 125028.
(38) Pfau, M. R.; McKinzey, K. G.; Roth, A. A.; Grunlan, M. A. PCL-Based Shape Memory Polymer Semi-IPNs: The Role of Miscibility in Tuning the Degradation Rate. *Biomacromolecules* **2020**, *21* (6), 2493−2501.
(39) Yi, F.; Xu, F.; Gao, Y.; Li, H.; Chen, D. Macrocellular polymer foams from water in oil high internal phase emulsion stabilized solely by polymer Janus nanoparticles: preparation and their application as support for Pd catalyst. *RSC Adv.* **2015**, *5* (50), 40227−40235.
(40) Gitli, T.; Silverstein, M. S. Emulsion templated bicontinuous hydrophobic-hydrophilic polymers: Loading and release. *Polymer* **2011**, *52* (1), 107−115.
(41) Cheu, C.; Yang, L.; Nieh, M.-P. Refining internal bilayer structure of bicelles resolved by extended-q small angle X-ray scattering. *Chem. Phys. Lipids* **2020**, *231*, 104945.
(42) Richter, A. G.; Dergunov, S. A.; Ganus, B.; Thomas, Z.; Pingali, S. V.; Urban, V.; Liu, Y.; Porcar, L.; Pinkhassik, E. Scattering Studies of Hydrophobic Monomers in Liposomal Bilayers: An Expanding Shell Model of Monomer Distribution. *Langmuir* **2011**, *27* (7), 3792−3797.
(43) Feigin, L. A.; Svergun, D. I.; Taylor, G. W., Principles of the Theory of X-Ray and Neutron Scattering. In *Structure Analysis by Small-Angle X-Ray and Neutron Scattering*, Feigin, L. A.; Svergun, D. I., Taylor, G. W., Eds.; Springer: Boston, MA, 1987; pp 3−24.
(44) Dubé, M. A.; Salehpour, S. Applying the Principles of Green Chemistry to Polymer Production Technology. *Macromol. React. Eng.* **2014**, *8* (1), 7−28.
(45) Langford, C. R.; Johnson, D. W.; Cameron, N. R. Chemical functionalization of emulsion-templated porous polymers by thiol-ene "click" chemistry. *Polym. Chem.* **2014**, *5* (21), 6200−6206.
(46) De Alwis Watuthanthrige, N.; Dunn, D.; Dolan, M.; Sparks, J. L.; Ye, Z.; Zanjani, M. B.; Konkolewicz, D. Tuning Dual-Dynamic Network Materials through Polymer Architectural Features. *ACS Applied Polymer Materials* **2022**, *4* (2), 1475−1486.
(47) Utroša, P.; Gradišar, S.; Onder, O. C.; Žagar, E.; Pahovnik, D. Synthetic Polypeptide-Polyester PolyHIPEs Prepared by Thiol-Ene Photopolymerization. *Macromolecules* **2022**, *55* (13), 5892−5900.
(48) Wang, Q.; Liu, Y.; Chen, J.; Du, Z.; Mi, J. Control of Uniform and Interconnected Macroporous Structure in PolyHIPE for Enhanced CO2 Adsorption/Desorption Kinetics. *Environ. Sci. Technol.* **2016**, *50* (14), 7879−7888.
(49) Li, H.; Yin, W.; Ng, C. K.; Huang, R.; Du, S.; Sharma, M.; Li, B.; Yuan, G.; Michalska, M.; Matta, S. K.; Chen, Y.; Chandrasekaran, N.; Russo, S.; Cameron, N. R.; Funston, A. M.; Jasieniak, J. J. Macroporous perovskite nanocrystal composites for ultrasensitive copper ion detection. *Nanoscale* **2022**, *14* (33), 11953−11962.

https://doi.org/10.1021/acsmacrolett.3c00255
ACS Macro Lett. 2023, 12, 993−998